The International Journal of Advanced Manufacturing Technology (2018) 96:1293–1304
https://doi.org/10.1007/s00170-018-1606-9

ORIGINAL ARTICLE

Predictive cutting force model for a cryogenic machining process incorporating the phase transformation of Ti-6Al-4V

Do Young Kim[1] · Dong Min Kim[1] · Hyung Wook Park[1]

Received: 27 October 2017 / Accepted: 10 January 2018 / Published online: 10 February 2018

Abstract

Titanium alloys have been attracting interest in aerospace industries because of their high strength-to-weight ratio. However, they are classified as difficult-to-machine materials due to poor tool life in machining processes. Cryogenic machining is a process that uses liquid nitrogen (LN2) as a coolant, and proposed as a method to enhance tool life in the present study. This paper presents a theoretical study to develop a predictive cutting force model for cryogenic machining of Ti-6Al-4V. A modified (in terms of cutting temperature) Johnson-Cook model that considers phase transformation, and a friction coefficient were used as input parameters for inclusion of the cryogenic cooling effect. The predictive cutting force model was validated based on an orthogonal cutting test. The predicted forces showed good agreement with the experimental data, with minimum and maximum error magnitudes of 1.9 and 17.7% for cutting force, and 0.3 and 32.8% for thrust force, respectively. Investigation of the effects of cryogenic cooling on the cutting force, micro-structure, surface integrity and burr height were conducted. The cutting force during cryogenic machining was increased compared to dry machining by a martensitic phase transformation of the work material. There was no effect of cooling condition on the surface roughness. The burr height under cryogenic conditions was decreased by 56.2 and 28.2% compared to the dry and wet conditions, respectively.

Keywords Titanium alloy · Cryogenic machining · Phase transformation · Predictive modeling

Nomenclature

σ	flow stress (MPa)
A	yield stress (MPa)
B	strain hardening coefficient
n	strain hardening exponent
C	strain rate coefficient
m	thermal coefficient
ε	plastic strain
$\dot{\varepsilon}^*$	dimensionless strain rate (s^{-1})
T^*	homologous temperature
ε_f	equivalent plastic strain to fracture
D_{1-5}	damage parameters
σ^*	dimensionless pressure-stress ratio
T_{shear}	simulated temperature at shear plane (°C)
$T_{shear,\ Dry}$	simulated temperature at shear plane in dry condition (°C)
$T_{shear,\ Cryogenic}$	simulated temperature at shear plane in cryogenic condition (°C)
T_{chip}	simulated temperature at surface of chip (°C)
r	cutting ratio
p_c	distance among teeth of chip (m)
p	height of teeth of chip (m)
β	tool face friction angle (rad)
μ	friction coefficient at tool-chip interface
H, h	phase constants
f_p	product volume fraction in phase transformation
k_p, n_p	JMA parameters
$t_{Cooling}$	cooling time, min

Research highlights We developed the predictive model of cryogenic machining with the phase transformation.
Experimental validations of FEM simulation and cutting forces were performed.
Martensitic phase transformation increases cutting forces at high cutting speed.
Cryogenic machining can improve the productivity by decreasing the burr height.

✉ Hyung Wook Park
hwpark@unist.ac.kr

[1] Department of Mechanical Engineering, Ulsan National Institute of Science and Technology, UNIST-gil 50, Eonyang-eup, Ulju-gun, Ulsan, Republic of Korea 689-798

T	temperature (°C)
$\dot{\gamma}$	shear flow strain rate at shear zone (min^{-1})
l	length of shear zone (m)
C_{Oxley}	strain rate constant for chip formation zone
V_S	shear velocity (m/min)
CR	cooling rate for phase transformation (°C/s)
F_C	cutting force (N)
F_T	thrust force (N)
k	shear flow stress at shear zone (Pa)
t_1	un-deformed chip thickness (m)
w	cutting width (m)
ϕ	shear angle (rad)
θ	slip-line field angle (rad)
λ	friction angle (rad)
α	rake angle (rad)

1 Introduction

Titanium and titanium alloys have been widely used in aerospace and medical industries due to their high strength-to-weight ratio, biocompatibility, and corrosion resistance [1, 2]. Among the various titanium alloys, Ti-6Al-4V is known to be the most common in these industries. During the machining process of Ti-6Al-4V, poor thermal properties, including a low specific heat, induce excessive heat generation during plastic deformation. The generated heat is not dissipated due to the low thermal conductivity of the material and the accumulated heat at the plastic deformation zone induces an increase of cutting tool temperature. Elevated temperature is an important parameter of tool wear and surface defects of the work material [3]. Accordingly, the Ti-6Al-4V alloy has been reported as a difficult-to-machine material during conventional cutting processes.

Traditional cutting fluids have been mainly applied in the machining of titanium alloys to improve machinability. However, in recent studies, a restriction of the cutting fluids has been required due to health and environmental hazards [4]. Cryogenic machining has been studied as an alternative method in previous research [5–7]. Cryogenic machining is an eco-friendly process using liquid nitrogen (LN2), which is non-toxic, as a coolant. Sprayed LN2 has a cryogenic temperature (− 196 °C), can reduce the cutting temperature [5], and has been proven to enhance tool life by decreasing tool temperature. Hong et al. [6] reported that tool life during cryogenic machining of Ti-6Al-4V alloy increased compared to conventional emulsion machining. However, the rapid change in temperature can lead to cold-strengthening and phase transformation of the work material during cryogenic machining [7, 8]. Ti-6Al-4V has a sequential combination of α (95 wt.%) + β (5 wt.%) phase at room temperature [8] and the micro-structural transition, including phase transformation of the target material, occurs at a high temperature above the recrystallization temperature. α to β phase transformation appears with an increase in temperature [8]. While Ti-6Al-4V is gradually cooled, the β phase begins to transform depending on the cooling rate. At a low cooling rate, the β to α phase transformation is induced by a diffusion-controlled nucleation approach [8–10]. A high cooling rate (> 410 °C/s) causes a martensitic transformation of β phase to α' phase, which is face-centered cubic (fcc) or face-centered tetragonal [11]. The cold-strengthening and martensitic phase transformation are potential factors in the cutting force increase. Hong et al. [7] reported that the cutting forces in the turning process are increased by the cold-strengthening effect during cryogenic machining. Jovanovic et al. [12] reported that under a rapid cooling rate, material tensile strength and hardness, which affect the cutting force, are enhanced by dynamic recrystallization (DRX).

Many researchers have focused on cutting force measurement during cryogenic machining [7, 13] and simulation models have been developed to predict the cutting force [14, 15]. Rotella et al. [15] performed a numerical simulation of the cutting force for aluminum alloy under cryogenic conditions. However, there has been no simulation study incorporating the phase transformation to predict cutting force during cryogenic machining. Because the Ti-6Al-4V alloy is sensitive to temperature, consideration of phase transformation is required for theoretical study. It is well known that a numerical approach is more accurate compared to an analytical approach in the simulation of cutting temperature. However, in the case of a finite element model (FEM), the simulation of phase transition according to each temperature analysis step is not adequate due to a lengthy processing time.

In this research, a predictive model for the cutting force during cryogenic machining of Ti-6Al-4V was developed by a combination of numerical and analytical methods. The predictive cutting force model included the cutting temperature, material constitutive model, and friction coefficient at a tool-chip interface as input parameters. The cutting temperature was simulated using FEM simulation and the simulated result was implemented to the analytical approach for predicting phase transition and cutting force. A modified Johnson-Cook model, which includes a phase constant, was adopted as the material constitutive model, and the friction coefficient was deducted using a chip morphology analysis. Then, validation of the predictive cutting force was performed using the experimental data of an orthogonal cutting test. To observe the phase transformation by cryogenic orthogonal machining, a micro-structural analysis was performed on the chip surface, which was generated by the machining experiment. Additionally, cryogenic effects on surface roughness and burr height were investigated.

2 FEM simulation of cutting temperature

During the cryogenic machining process, the sprayed LN2 can reach the surface of the work material; the temperatures of the chip and work material are reduced by the convective effect of the LN2. Numerical modeling is an adequate method to simulate heat convection. In this section, a two-dimensional FEM simulation was carried out using the ABAQUS explicit program to predict the cutting temperatures under dry and cryogenic conditions. The simulated temperatures were applied to the predictive cutting force model and the overall procedure of the numerical and analytical studies is described in Fig. 1.

2.1 Material constitutive model

A plasticity model can represent the flow stress induced by plastic deformation of the work material in the FEM simulation. In this research, the Johnson-Cook model, which is the most popular empirical model due to the advantages of simple form and small calculation quantity [16], was adopted as the plasticity model. The material model is shown in Eq. (1)

$$\sigma = (A + B\varepsilon^{n})\left(1 + C\ln\dot{\varepsilon}^{*}\right)\left(1 - T^{*m}\right) \quad (1)$$

where σ is the flow stress, A is a yield stress, B is a strain hardening coefficient, n is a strain hardening exponent, C is a strain rate coefficient, m is a thermal coefficient, and ε is a plastic strain.

The material constitutive model includes the five parameters (A, B, n, C, m); to obtain the parameters, a tension test was carried out under a large range of strain rates (0.0001–0.1 s^{-1}) and temperature (25–600 °C). Under all the strain rate and temperature conditions, a material tester (INSTRON, 5982 Type) was used and the ASTM D 638 type specimen was adopted. The computed parameters are shown in Table 1. In earlier research, five parameters for the Johnson-Cook model were achieved under various testing conditions [17–19]. The computed parameters showed similar trends to the reported parameters, and it was confirmed that the computed parameters are suitable for application to the FEM simulation.

2.2 Boundary condition of the FEM simulation

The mesh and boundary conditions are shown in Fig. 2. A round-edged tool with a nose radius of 76 μm was used. After the pre-machining test, the tool edge radius was measured by contour analysis using a surface profiler (Mitutoyo, 525–421 k^{-1}). The tool and work materials were tungsten carbide and Ti-6Al-4V. The cutting tool was applied as a rigid body part and a 0.1-mm depth of cut was used. Velocities of the bottom and left sides of the work material were set as zero and the cutting tool moved with cutting speeds of 90, 150, and 210 m/min. The initial temperatures of the work material were set to 25.6 and − 179.6 °C under dry and cryogenic conditions, respectively. The temperatures of air and sprayed LN2 were measured using a K-type thermocouple and the measured data were applied to the initial temperatures. At the top side of the work material, heat convective coefficients of 25 and 50×10^{7} W/m^2-K were applied under dry and cryogenic conditions, respectively [20]. Input temperatures for the heat convection were set to the measured temperatures in each cooling condition. Four-node plane strain thermally coupled quadrilateral, bilinear displacement and temperature, reduced integration, hourglass control (CPE4RT) elements were applied to the work material and cutting tool. A damage criterion of the Johnson-Cook model was employed as follows:

$$\varepsilon_f = \left[D_1 + D_2\exp\left(D_3\sigma^{*}\right)\right]\left[1 + D_4\ln\dot{\varepsilon}^{*}\right]\left[1 + D_5T^{*}\right] \quad (2)$$

where ε_f is an equivalent plastic strain to fracture, and D_1–D_5 are damage parameters. The D_1–D_5 are possible to quantify of the ability to maintain plastic deformation and they can be obtained by a fundamental material test to fracture. The damage parameters, which were obtained from previous research, were used [21]. Properties of Ti-6Al-4V, which were applied to the simulation, are shown in Tables 1, 2, and 3.

The temperatures at the shear band and chip surface were simulated. In the meshed work material, nodes positioned at the shear band and chip surface were selected and cutting temperatures were obtained at the nodes. The selected nodes can be observed in Fig. 2. Average node temperatures were used as cutting temperatures at shear band (T_{shear}) and chip surface (T_{chip}). In cryogenic machining, the cryogenic cooling process affects the variation in chip morphology, and the morphology can represent the cutting mechanism [13]. The simulation result was validated using chip morphology analysis and the results of the simulation and validation are presented in Section 5.1.

3 Predictive cutting force modeling

An analytical approach was used to predict the cutting force during cryogenic machining. The cutting temperature, friction coefficient at the tool-chip interface and material constitutive model, which includes a phase constant, were considered in the proposed prediction model to reflect the cryogenic cooling effect. A flow chart of the cutting force prediction is described in Fig. 1.

3.1 Friction coefficient at the tool-chip interface

During the cryogenic machining process, reduction of temperature due to LN2 can induce a change in the friction coefficient at the tool-chip interface. When a serrated chip is generated by titanium machining, the geometry of the chip depends

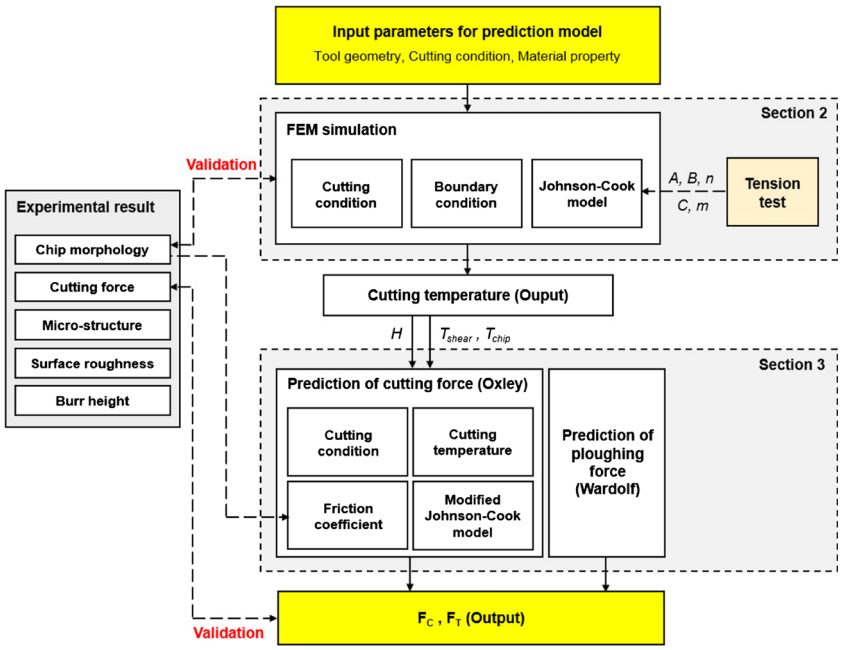

Fig. 1 Flow chart of a predictive cutting force model of the cryogenic machining process for Ti-6Al-4V alloy

on the friction coefficient. Vyas et al. [22] reported a relationship between the friction coefficient and morphology of the saw-tooth chip. Methods for calculating the friction coefficient according to the chip shape have been reported for metals, including titanium alloys [22–24]. In this study, the theoretical coefficient of sliding friction was computed by a chip morphology analysis under various cutting conditions. Equations were applied as follows:

$$r = \frac{p_c}{p} \tag{3}$$

$$\phi = \tan^{-1}\left(\frac{r\cos\alpha}{1 + r\sin\alpha}\right) \tag{4}$$

$$\phi = \frac{\pi}{4} - \frac{\beta}{2} + \frac{\alpha}{2} \tag{5}$$

$$\mu = \tan\beta \tag{6}$$

where r is the cutting ratio, P_C is the distance among the teeth of the chip, P is the height of the teeth of the chip, β is the tool face friction angle, and μ is the friction coefficient at the tool-chip interface.

Descriptions of the input parameters of the computation representing the geometry of a serrated chip were given previously [22]. Average friction coefficients under each cooling condition were used as representative values in this study and applied to the predictive cutting force model.

Table 1 Johnson-Cook model parameters of Ti-6Al-4V

Parameter	A	B	n	C	m
Value	856.41	840.26	0.880	0.011	0.663

3.2 Determination of the phase constant representing martensitic transformation

The original Johnson-Cook model cannot represent mechanical property changes according to phase transformation [16]. In this section, to predict the cutting force during cryogenic machining process, a modified Johnson-Cook model, which includes a phase constant, H, was proposed. The material model is based on the plasticity model reported by Seo et al. [25], and the basic form is as follows:

$$\sigma = (A + B\varepsilon^n)\left(1 + C\ln\dot{\varepsilon}^*\right)\left(1 - T^{*m}\right)H \tag{7}$$

where H is the phase constant.

The reported plasticity model includes the phase constant, which has a simple form not including the kinematics of the phase transformation. On the other hand, in this paper, the Johnson-Mehl-Avrami (JMA) model was applied to calculate the volume fraction of the martensitic phase transformation. The JMA is a representative model of the phase transformation kinematics [26, 27]. In Gil Mur et al. [28], input parameters of the JMA model were deduced for the martensitic phase transformation of Ti-6Al-4V under various temperatures. In this work, empirical equations including temperature as a variable were constructed by using the reported JMA parameters, and the equations were applied to the proposed material constitutive model. A formula including the relationship between the phase constant and the JMA model is

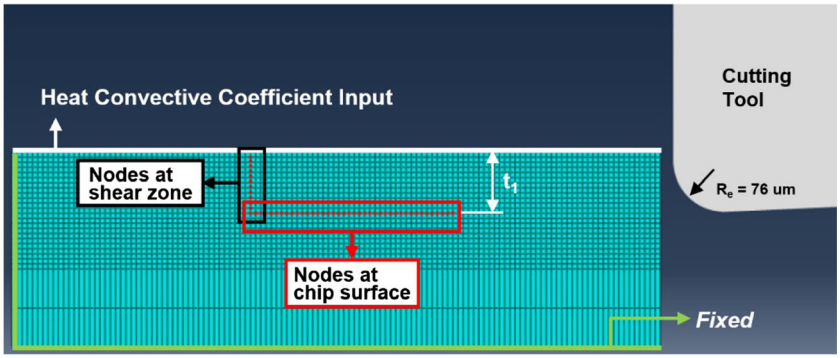

Fig. 2 Boundary condition of a finite element model (FEM) simulation of cutting temperature

provided in Eq. (8), and the basic form of the JMA model is shown in Eq. (9). The empirical equations and reported data are summarized in Eqs. (10) and (11), and in Table 4. In general, to obtain the volume fraction of phase transformation, a specific cooling time is required [8, 29]. However, for the machining process, it is hard to characterize the cooling time because the chip is continuously generated in an extremely short time. In this research, it was assumed that the phase transformation is processed at the narrow shear band, with intense shear concentration, because the cutting temperature begins to rise at the shear zone by the primary heat source. Yan et al. [30] reported that the shear strain rate is strongly correlated with the time for shear concentration in the chip formation of titanium alloys. Therefore, a reciprocal of the shear strain rate was applied as the cooing time in the JMA model and the cooling time is described in Eq. (12).

$$H = 1 + f_p h \tag{8}$$

$$f_p = 1 - \exp\left(-k_p {t_{Cooling}}^{n_p}\right) \tag{9}$$

$$n_p = 0.0021T - 0.0799 \tag{10}$$

$$k_p = 0.00004T - 00021 \tag{11}$$

$$t_{Cooling} = \frac{1}{\dot{\gamma}} = \frac{l}{C_{Oxley} V_S} \tag{12}$$

where h is the phase constant, f_p is the product volume fraction during phase transformation, n_p and k_p are the JMA parameters, T is the temperature, and $t_{Cooling}$ is the cooling time.

After the martensitic phase transformation, the tensile strength of the target material changes according to the cooling rate. Filip et al. [31] reported an experimental study showing a change in the yield stress of Ti-6Al-4V according to variation in the cooling rate; there was a linear relationship between the yield stress and cooling rate. The yield stress correlates with the flow stress during plastic deformation of the work material. In this research, a linear equation representing that relationship was constructed to obtain the phase constant, h, and is shown in Eq. (13).

$$h = 0.0039CR + 0.0009 \tag{13}$$

where CR is the cooling rate for phase transformation.

To obtain the cooling rate, the FEM simulation results for the cutting temperature at the shear plane were used. Because the time for chip generation is short, it was assumed that the initial temperature at the shear band during cryogenic machining is the same as $T_{shear,Dry}$, and that the temperature is decreased by cryogenic cooling. The cooling rate was computed according to the difference between $T_{shear,\ Dry}$ and $T_{shear,\ Cryogenic}$, and the cooling rate is described in Eq. (14). The constructed parameters under various cutting speeds were applied to the material model.

$$CR = \frac{\left(T_{shear,Dry} - T_{shear,Cryogenic}\right)}{60 \cdot t_{Cooling}} \tag{14}$$

3.3 Cutting force model

The Oxley model is a cutting force prediction model using a slip-line method [34]. To predict cutting force, the Oxley model incorporates the cutting tool geometry and properties of the work material. During the machining process, plastic deformation of the work material occurs and a flow stress is induced according to the mechanical properties of the material

Table 2 Damage parameters of Ti-6Al-4V alloy

Parameter	D_1	D_2	D_3	D_4	D_5
Value	−0.09	0.25	−0.5	0.014	3.87

Table 3 Properties of Ti-6Al-4V alloy

Parameter	Value
Modulus of elasticity (GPa)	110
Poisson's ratio	0.41
Specific heat (J/kg-°C)	580
Thermal conductivity (W/m-°C)	7.3
Density (kg/m^3)	4428
CTE (um/m-°C)	9.2
Melting temperature (°C)	1632

Table 4 Parameters for Avrami model in difference temperatures

T (°C)	n_p	k_p
400	0.667	0.0192
500	1.106	0.0147
600	1.252	0.0246
700	1.326	0.0307

and the cutting conditions. The mechanical properties depends on the temperature. Then, the cutting force (F_C) and thrust force (F_T) are calculated by considering the flow stress and tool geometry, which includes the rake and inclination angles. The forces can be deducted by multiplication of the flow stress and cutting area at the shear zone. F_C and F_T are presented in Eqs. (15) and (16) [32].

$$F_C = \frac{kt_1 w}{\sin\phi\cos\theta}\cos(\lambda-\alpha) \tag{15}$$

$$F_T = \frac{kt_1 w}{\sin\phi\cos\theta}\sin(\lambda-\alpha) \tag{16}$$

where k is the shear flow stress, t_1 is an un-deformed chip thickness, and w is the cutting width.

A predictive cutting force model for the cryogenic orthogonal cutting process was developed in MATLAB based on the Oxley model. Under cryogenic conditions, the cutting temperature and mechanical properties of the work material are changed by spraying of LN2. The cutting temperature simulated by the FEM model was applied to obtain the mechanical properties of a target material, and the flow stress and cutting force were determined considering the cutting conditions and properties of the work material. During the cutting process, the tip of the tool presses the work material and this phenomenon induces a plowing effect. Wardolf et al. [33] reported that an additional cutting force, i.e., a plowing force, is caused by the plowing effect. The result of the predictive model was computed by summing the cutting force, which is based on the Oxley model, and the plowing force.

4 Experimental setup

An orthogonal cutting experiment was carried out for the Ti-6Al-4V material using a lathe machine (S&T, TSL 6). A disc-type specimen was used. The test was executed with a feed of 0.1 mm/rev, cutting width of 1 mm, and various cutting speeds (90, 150, 210 m/min). During the machining of titanium alloys, the cutting temperature is the main parameter determining the machinability. Because the cutting speed has a significant effect on the cutting temperature relative to the feed and cutting width, a large range of cutting speeds were applied during the test. The experimental conditions are shown in Table 5 and Fig. 3. Three cooling conditions (dry, wet, cryogenic) were applied throughout the experiment. Under wet and cryogenic conditions, conventional oil and LN2 were adopted as coolants, respectively, and a tool holder supporting the coolants during internal passage was used (SANDVIK). The tool holder includes two holes having a diameter of 1 mm to release the coolants. The coolants were sprayed heading to rake and flank faces of the tool insert. The pressure of the LN2 was fixed as 15 bars under cryogenic conditions. To eliminate any effect of the coating material, an uncoated tungsten carbide tool insert (SANDVIK), which has rake and inclination angles of zero degrees, was applied.

Table 5 Experimental conditions for the orthogonal cutting test of the Ti-6Al-4V alloy

Cooling condition	Cutting speed (m/min)	Cutting width (mm)	Feed (mm/rev)
Dry Wet Cryogenic	90, 150, 210	1	0.1

Before performing the experiment, pre-machining was conducted to achieve a planar surface on the work material. During the machining process, a force dynamometer (KISTLER, 9257B) was applied to measure the cutting force and the tool holder was attached to the dynamometer. To prevent thermal shock of the dynamometer by LN2, a Teflon plate was placed between the tool holder and dynamometer.

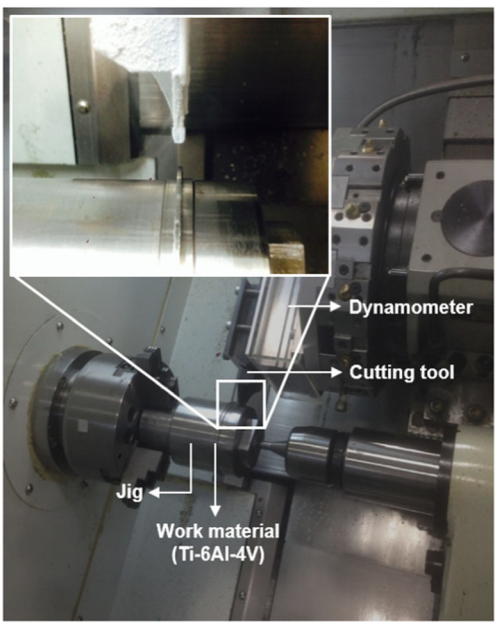

Fig. 3 Experimental setup of the cryogenic orthogonal cutting experiment

5 Result and discussion

5.1 FEM validation and chip morphology analysis

In the case of machining of Ti-6Al-4V, a serrated chip was generated, and the chip morphology is determined by the property of work material and the machining condition which includes the cooling effect of coolants [13]. Many previous researches have analyzed the mechanism of serrated chip as theories of adiabatic shear band and cyclic crack propagation [22, 34, 35], and it was reported that the chip formation has a great influence on the distribution of cutting temperature [35, 36]. In this study, the shape of the chip was used to validate the cutting temperature which was simulated by the FEM model. Chip height (H_{chip}) and the distance between the teeth of the chip (D_{chip}) were compared between experimental and simulated chip shapes at cutting speeds of 90, 150, and 210 m/min. The chip morphology was measured using a scanning electron microscope (FEI, Nova Nano). The simulated chip morphology matched well to the experimental results, with minimum and maximum error magnitudes of 0.3 and 8.4% for H_{chip}, and 0.7 and 8.8% for D_{chip}, respectively (Fig. 4). This result proves that the simulated cutting temperature is adequate in the predictive cutting force model.

The simulation results of cutting temperature are summarized in Table 6. Under cryogenic conditions, negative temperatures occurred at nodes near to the convection layer, and the cutting temperatures (T_{shear}, T_{chip}) under cryogenic conditions were lower than those under dry conditions, due to the effect of LN2. With the increase in cutting speed, the cutting temperatures were increased and the difference between the shear zone temperature under dry and cryogenic conditions showed a positive relationship with cutting speed.

Computation of the friction coefficient at the tool-chip interface was performed and the results are shown in Table 7. The friction coefficients under cryogenic conditions were lower than those under dry and wet conditions. Due to LN2 being sprayed on to the tool rake face, adhesion at the tool-chip interface can be reduced [37]. The decrease in the friction coefficients may have been caused by the reduction of adhesion. The effect of cooling on the friction coefficient was significant relative to the cutting speed; thus, it appears that the cooling condition is a dominant parameter in the friction coefficient.

5.2 Validation of the predictive cutting force model and cutting force analysis

Cutting force prediction was performed under three different cooling conditions. The cutting temperature, material constitutive model, and friction coefficient were used as input parameters. Under wet conditions, it was assumed that the effect of the conventional oil on cutting temperature could be ignored, because the rate of increase in cutting temperature is extremely high relative to the temperature of the oil (24.3 °C) and cutting temperatures simulated under dry conditions were applied. The temperature of the oil was measured using a K-type thermocouple. Under cryogenic conditions, the computed phase constants were applied to the material model, whereas a constant of 1 was applied to the H value under dry and wet conditions. Predictive cutting forces were validated by experimental data and the results are shown in Fig. 5. The validation result showed good agreement between the predicted and experimental cutting forces, with minimum and maximum error magnitudes of 1.9 and 17.7% for F_C, and 0.3 and 32.8% for F_T, respectively. To confirm the effect of the phase constant under cryogenic conditions, a comparison between predictive forces with and without the phase constant was performed. The results of the comparison are shown in Fig. 6. When the phase transformation was considered, the reliability of the model was increased in terms of F_T. Thus, it can be concluded that analysis of phase transformation is necessary to predict the cutting mechanism of the Ti-6Al-4V under cryogenic conditions.

Regarding the orthogonal cutting process, the measured cutting forces are summarized in Fig. 5. At low cutting speeds (90–150 m/min), there was no significant difference in cutting force according to the cooling conditions. Under cryogenic conditions, a decrease in cutting temperature was observed in the FEM simulation, which elevated the cutting force. However, it appears that the decrease in friction coefficient caused by cryogenic cooling may attenuate the cold-strengthening effect. Conversely, at a high cutting speed (210 m/min), a drastic increase in cutting force was detected due to cryogenic cooling. Under cryogenic conditions, martensitic phase transformation can occur via rapid heating and cooling. Under high cutting speed conditions, the maximum cutting temperature and cooling rate can be generated, and it appears that the increase of force is due mainly to the phase transformation.

In the predicted cutting forces, there are severe discrepancies for some cutting conditions. The causes of the discrepancies may be accounted for the effects of property of work material, tool vibration, and cutting tool wear. In this study, the cutting temperature and the mechanical property of work material were computed in a steady state of machining process. However, during the cryogenic machining process, the LN2 is sprayed to a localized region of the work material, and irregularities in the material temperature and work material property may appear. Further, the cutting tool may vibrate due to the cutting force in feed direction, and the vibration can induce the variations of cutting depth and machining force. In a machining process, an occurrence of flank wear can induce the deformation of cutting tool shape and the variation of cutting force. However, in the analytical process, it was assumed that the tool wear could be ignored, due to short machining distance. In the comparison result, the maximum error magnitude occurred at the cutting speed of 210 m/min, and it can be considered that

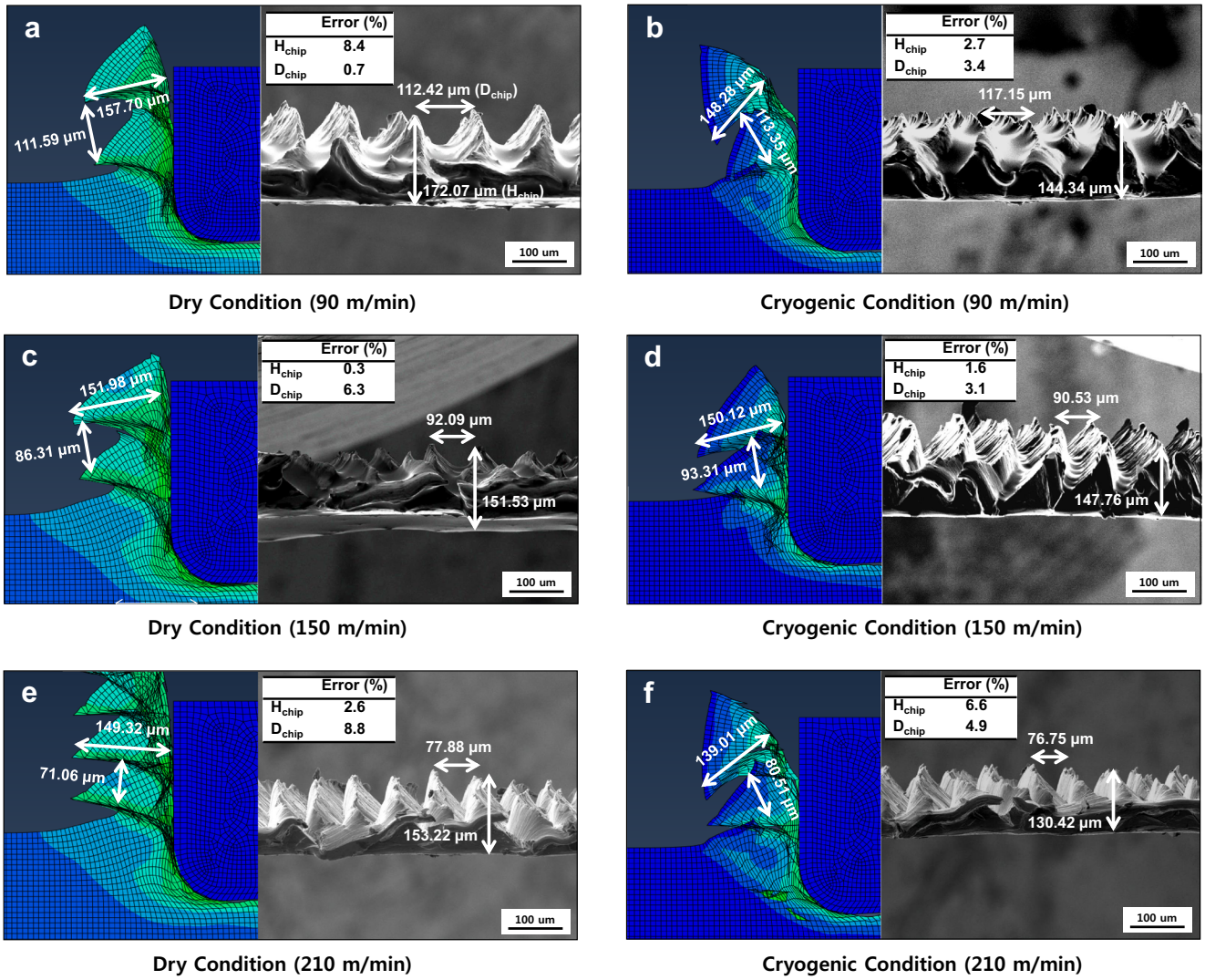

Fig. 4 Comparison between simulated and measured chip morphologies under dry (**a**, **c**, **e**) and cryogenic (**b**, **d**, **f**) conditions at cutting speeds of 90, 150, and 210 m/min

the main cause of the discrepancy is the effect of tool wear because a high cutting temperature, which is a factor of the tool wear, is generated in high speed machining processes. The proposed predictive model is required to be further developed by accounting for the existence of cutting tool wear effect.

5.3 Micro-structural analysis (phase transformation)

In the predictive model, the phase transformation was incorporated to predict the cutting force under cryogenic conditions. To confirm the occurrence of martensitic phase transformation, a micro-structural analysis was carried out using X-ray diffraction (XRD) analysis on the surface of the generated chip from the cryogenic orthogonal cutting test. XRD is a method for analyzing micro-structure, including the phase of the target material. It can represent the phase combination by a peak pattern. In the case of Ti-6Al-4V, when the martensitic transformation occurs, a shift in the XRD peak, which is matched to an α (101) phase, is induced and the shifted peak angle has a positive correlation with the volume

Table 6 Simulated cutting temperatures at the shear band and chip surface

Cooling condition	T_{shear} (°C)			T_{chip} (°C)		
	90 m/min	150 m/min	210 m/min	90 m/min	150 m/min	210 m/min
Dry	474.8	508.0	534.9	679.0	685.0	742.6
Cryogenic	279.8	297.8	298.8	506.0	562.3	579.4

Table 7 Computed friction coefficients at the tool-chip interface: chip morphology analysis

Cooling condition	Friction coefficient			Average value
	90 m/min	150 m/min	210 m/min	
Dry	0.52	0.57	0.56	0.55
Wet	0.50	0.46	0.46	0.47
Cryogenic	0.48	0.43	0.41	0.44

fraction of phase transformation. Jovanovic et al. [12] conducted an XRD analysis for a water-quenched Ti-6Al-4V alloy and confirmed a shift in the XRD peak by martensitic phase transformation. A high power XRD (Rigaku, D/MAX-2500 V) was applied for the analysis by using graphite monochromated Cu Kα radiation with 200 mA current and 40 kV of operating voltage. The X-ray was scattered on the overall area of target material, chip surface, and an

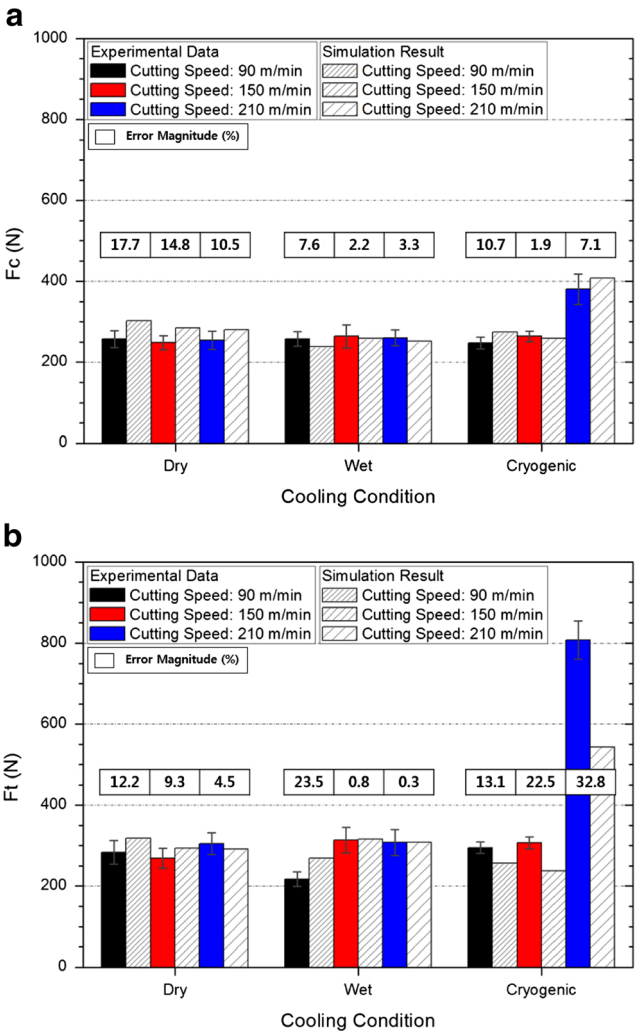

Fig. 5 Validation of predictive cutting forces based on experimental data in the **a** F_c and **b** F_t force directions

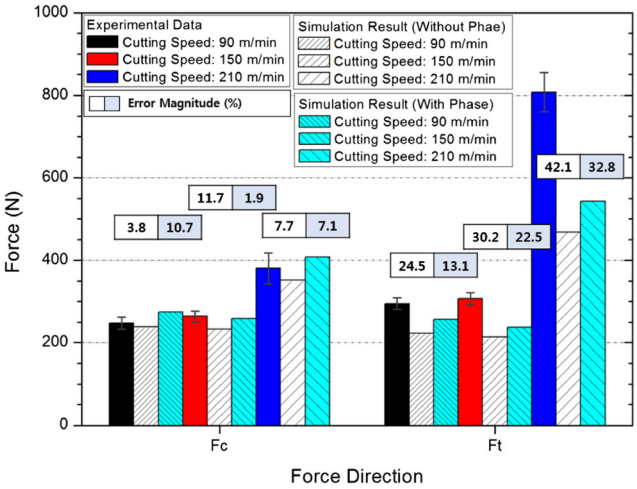

Fig. 6 Comparison between predictive cutting forces with and without phase constant

average phase combination was detected. The analysis was performed for three different samples in each cutting condition, and the results of the micro-structural analysis with a schematic diagram of the diffraction pattern are described in Fig. 7. Martensitic transformations were detected at cutting speeds of 90–210 m/min and the maximum shifted angle of the XRD peak was found at a cutting speed of 210 m/min. This proves that the martensitic phase transformation led to a drastic increase in cutting force at the 210 m/min cutting speed. On the other hand, with a 150 m/min cutting speed, the minimum shifted XRD angle was detected. When the cutting speed increases, the cooling rate is increased, while the cooling time for phase transformation is decreased. The conflicting parameters cause a non-linear relationship between the cutting speed and volume fraction of phase

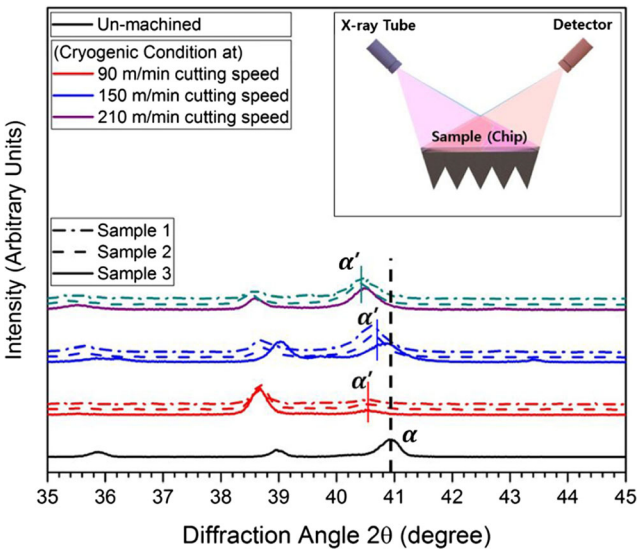

Fig. 7 Experimental result of X-ray diffraction (XRD) analysis of the chip surface generated by a cryogenic orthogonal cutting test

transformation, which may induce the minimum shifted XRD angle at a 150 m/min cutting speed. It seems that application of a 150 m/min cutting speed is adequate to prevent the effect of martensitic phase transformation on the cutting force during cryogenic machining of a Ti-6Al-4V alloy.

5.4 Surface roughness

Surface roughness is the main parameter determining the quality of a product, and it is well known that the surface roughness depends on the cutting conditions [38]. To confirm the effects of cryogenic cooling on surface quality, the roughness of the work material was measured by machining under cryogenic cooling conditions by using the surface profiler (Mitutoyo, 525–421 k^{-1}). The measured data are summarized in Fig. 8 based on the surface roughness under dry conditions. Under wet and cryogenic conditions, the average surface roughness decreased by 9.2 and 11.8%, respectively. When a coolant is applied during the machining process, the reduced friction coefficient can improve the surface quality, and the effects of conventional oil and LN2 may reduce the surface roughness. However, within the measured data, the difference in roughness results according to cooling conditions seems to be small relative to the standard deviation for each cutting condition. Thus, it appears that the effect of martensitic phase transformation on the surface roughness is small.

5.5 Burr height

A side burr is one of the most common types of burr used during the orthogonal cutting process, and the height of the burr depends on the temperature of the work material [39, 40]. An increase in temperature induces an increase in burr height. In this study, burr heights of machined work materials

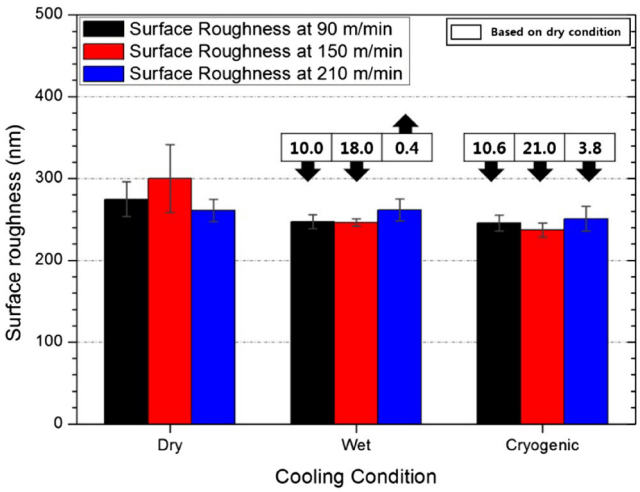

Fig. 8 Measured surface roughness results for machined surfaces of Ti-6Al-4V alloy under various cutting conditions

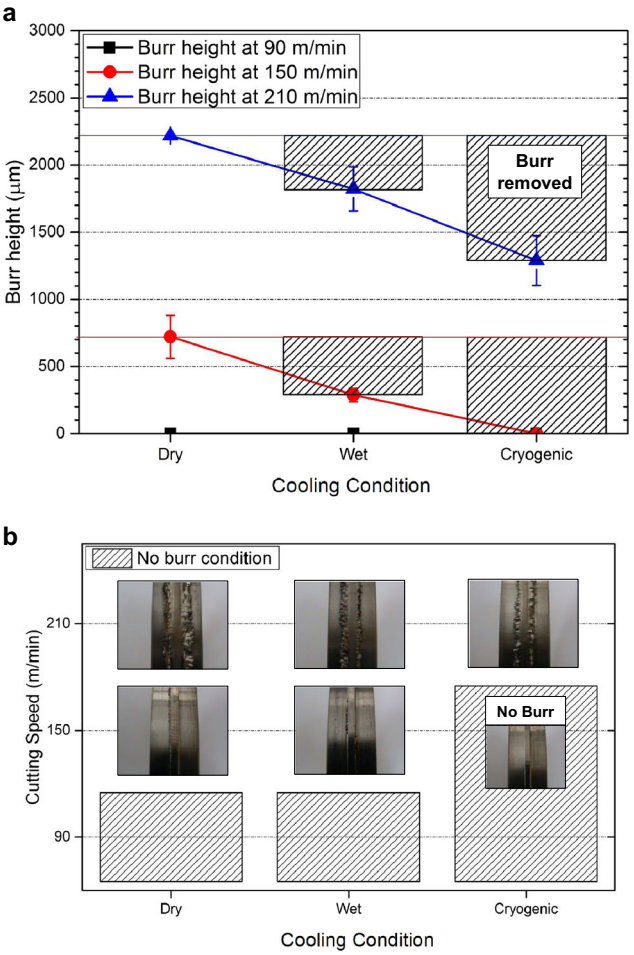

Fig. 9 **a** Measured burr height, and **b** qualities of the machined area shown by orthogonal cutting experiments under different cutting conditions

were measured using a laser scanning confocal microscope (Olympus, OLS-3100). The experimental results are shown in Fig. 9a. The average burr height under cryogenic conditions was decreased by 56.2 and 28.2% compared to the dry and wet conditions, respectively. Under cryogenic conditions, a drastic reduction in burr height was detected and it seems that the decrease in cutting temperature due to use of sprayed coolants in turn reduces burr height. At a cutting speed of 90 m/min, no burr was seen under any cooling conditions; the burr began to be generated at a cutting speed of 150 m/min. Under cryogenic conditions, no burr was seen at a cutting speed of 150 m/min. The qualities of machined surfaces according to the cutting conditions are presented in Fig. 9b. During the machining of titanium alloys, cutting speeds lower than 100 m/min have generally been applied. The range of cutting speeds depends on the machinability, for example in terms of tool life and product quality. When cryogenic coolant is applied during the machining of titanium alloys, it is expected that productivity will be enhanced by an increase in cutting speed.

6 Conclusion

In this study, a predictive force modeling for cryogenic machining was studied by a combination of the numerical and analytical approaches. Validation of the model was done using experimental data. The detailed conclusions are as follows:

(1) Cutting temperatures at the shear zone and chip surface were simulated under dry and cryogenic conditions by the FEM model. The simulated temperature under cryogenic conditions was lower compared to that under dry conditions. The simulation result was verified based on chip morphology analysis. The simulated chip shape matched well to the experimental data, with minimum and maximum error magnitudes of 0.3 and 8.4% for H_{chip}, and 0.7 and 8.8% for D_{chip}, respectively.

(2) The friction coefficient at the tool-chip interface under cryogenic conditions was decreased compared to that under dry and wet conditions. It seems that the reduction in adhesion at the tool rake face led to the decrease in the friction coefficient. Cooling was a dominant factor affecting the friction relative to the cutting speed.

(3) A predictive cutting force model for cryogenic machining of Ti-6Al-4V was developed and validated based on experimental data. A comparison between the predicted and experimental cutting forces was conducted and showed good agreement with the minimum and maximum error magnitudes of 1.9 and 17.7% for F_C, 0.3 and 32.8% for F_T. The prediction results showed a similar trend with the experimental results at cutting speeds of 90–210 m/min. A drastic increase in cutting force was induced by the martensitic phase transformation under cryogenic conditions with a high cutting speed (210 m/min). It can be concluded that consideration of phase transformation is necessary to predict the cutting force during cryogenic machining of Ti-6Al-4V.

(4) XRD analysis was performed on the chip surface, which was generated by the cryogenic orthogonal cutting test. The minimum volume fraction of the martensitic phase transformation was detected at a 150 m/min cutting speed. It can be concluded that a cutting speed of 150 m/min is adequate to prevent phase transformation and an increase in cutting force.

(5) There was no significant effect of cooling conditions on surface roughness. The burr height under cryogenic conditions was decreased by 56.2 and 28.2% compared to the dry and wet conditions, respectively. Especially, at a cutting speed of 150 m/min, no burr was present. It seems that the reduction in cutting temperature caused by LN2 spraying in turn caused the decrease in burr height. During conventional machining of titanium alloys, the cutting speed is limited to lower than 100 m/min due to poor machinability. In cryogenic machining, it is expected that productivity will improve due to the increase in cutting speed up to 150 m/min.

Acknowledgments This research was supported by the development of liquid nitrogen-based cryogenic machining technology and system for titanium and CGI machining funded by the Ministry of Trade, Industry & Energy (MOTIE) of Korea (No. 10048871) and the National Research Foundation of Korea (NRF) Grant funded by the Ministry of Science and ICT (NRF-2017R1A5A1015311).

References

1. Castellani C, Lindtner RA, Hausbrandt P, Tschegg E, Stanzl-Tschegg SE, Zanoni G, Beck S, Weinberg AM (2011) Bone–implant interface strength and osseointegration: biodegradable magnesium alloy versus standard titanium control. Acta Biomater 7(1): 432–440. https://doi.org/10.1016/j.actbio.2010.08.020
2. Long M, Rack H (1998) Titanium alloys in total joint replacement—a materials science perspective. Biomaterials 19(18):1621–1639. https://doi.org/10.1016/S0142-9612(97)00146-4
3. Che-Haron C (2001) Tool life and surface integrity in turning titanium alloy. J Mater Process Technol 118(1-3):231–237. https://doi.org/10.1016/S0924-0136(01)00926-8
4. Shokrani A, Dhokia V, Newman ST (2012) Environmentally conscious machining of difficult-to-machine materials with regard to cutting fluids. Int J Mach Tools Manuf 57:83–101
5. Hong SY, Ding Y (2001) Cooling approaches and cutting temperatures in cryogenic machining of Ti-6Al-4V. Int J Mach Tools Manuf 41(10):1417–1437. https://doi.org/10.1016/S0890-6955(01)00026-8
6. Hong SY, Markus I, Jeong WC (2001) New cooling approach and tool life improvement in cryogenic machining of titanium alloy Ti-6Al-4V. Int J Mach Tools Manuf 41:2245–2260
7. Hong SY, Ding Y, Jeong WC (2001) Friction and cutting forces in cryogenic machining of Ti–6Al–4V. Int J Mach Tools Manuf 41: 2271–2285
8. Sha W, Malinov S (2009) Titanium alloys: modelling of microstructure, properties and applications, Elsevier
9. Malinov S, Guo Z, Sha W, Wilson A (2001) Differential scanning calorimetry study and computer modeling of β⇒ α phase transformation in a Ti-6Al-4V alloy. Metall Mater Trans A 32(4):879–887. https://doi.org/10.1007/s11661-001-0345-x
10. Kherrouba N, Bouabdallah M, Badji R, Carron D, Amir M (2016) Beta to alpha transformation kinetics and microstructure of Ti-6Al-4V alloy during continuous cooling. Mater Chem Phys 181:462–469
11. Ahmed T, Rack H (1998) Phase transformations during cooling in α+ β titanium alloys. Mater Sci Eng A 243(1-2):206–211. https://doi.org/10.1016/S0921-5093(97)00802-2
12. Jovanović M, Tadić S, Zec S, Mišković Z, Bobić I (2006) The effect of annealing temperatures and cooling rates on microstructure and mechanical properties of investment cast Ti–6Al–4V alloy. Mater Des 27(3):192–199. https://doi.org/10.1016/j.matdes.2004.10.017
13. Bermingham M, Kirsch J, Sun S, Palanisamy S, Dargusch M (2011) New observations on tool life, cutting forces and chip morphology in cryogenic machining Ti-6Al-4V. Int J Mach Tools Manuf 51:500–511
14. Outeiro J, Rossi F, Fromentin G, Poulachon G, Germain G, Batista A (2013) Process mechanics and surface integrity induced by dry and cryogenic machining of AZ31B-O magnesium alloy. Procedia CIRP 8:487–492. https://doi.org/10.1016/j.procir.2013.06.138

15. Rotella G, Umbrello D (2014) Numerical simulation of surface modification in dry and cryogenic machining of AA7075 alloy. Procedia CIRP 13:327–332. https://doi.org/10.1016/j.procir.2014.04.055
16. Johnson GR, Cook WH (1983) A constitutive model and data for metals subjected to large strains, high strain rates and high temperatures. Proceedings of the 7th international symposium on ballistics, Netherlands. 541-547
17. Lesuer D (1999) Experimental investigation of material models for Ti-6Al-4V and 2024-T3. Livermore: University of California, Lawrence Livermore National Laboratory 1–36
18. Nemat-Nasser S, Guo WG, Nesterenko VF, Indrakanti S, Gu YB (2001) Dynamic response of conventional and hot isostatically pressed Ti–6Al–4V alloys: experiments and modeling. Mech Mater 33(8):425–439. https://doi.org/10.1016/S0167-6636(01)00063-1
19. Johnson G, Holmquist T (1989) Test data and computational strength and fracture model constants for 23 materials subjected to large strains, high strain rates, and high temperatures. Los Alamos National Laboratory, Los Alamos, NM, report no. LA-11463-MS
20. Shen N, Ding H, Gao J (2015) Cryogenic cutting of AZ31B-O Mg alloy for improved surface integrity–part II: physics-based process modeling of surface microstructural alteration. Proc of ASME 2015 International Manufacturing Science and Engineering Conference
21. Bajpai V, Lee I, Park HW (2014) Finite element modeling of three-dimensional milling process of Ti–6Al–4V. Mater Manuf Process 29(5):564–571. https://doi.org/10.1080/10426914.2014.892618
22. Vyas A, Shaw M (1999) Mechanics of saw-tooth chip formation in metal cutting. J Manuf Sci Eng Trans ASME 121(2):163–172. https://doi.org/10.1115/1.2831200
23. Stephenson D, Agapiou J (2005) Metal cutting theory and practice. Taylor & Francis, New York
24. Kim DM, Lee I, Kim SK, Kim BH, Park HW (2016) Influence of a micropatterned insert on characteristics of the tool–workpiece interface in a hard turning process. J Mater Process Technol 229:160–171. https://doi.org/10.1016/j.jmatprotec.2015.09.018
25. Seo S, Min O, Yang H (2005) Constitutive equation for Ti–6Al–4V at high temperatures measured using the SHPB technique. Int J Impac Eng 31:735–754
26. Johnson WA (1939) Reaction kinetics in process of nucleation and growth. Trans AIME 135:416–458
27. Malinov S, Markovsky P, Sha W, Guo Z (2001) Resistivity study and computer modelling of the isothermal transformation kinetics of Ti–6Al–4V and Ti–6Al–2Sn–4Zr–2Mo–0.08 Si alloys. J Alloys Compd 314(1-2):181–192. https://doi.org/10.1016/S0925-8388(00)01227-5
28. Mur FG, Rodriguez D, Planell J (1996) Influence of tempering temperature and time on the α′-Ti-6Al-4V martensite. J Alloys Compd 234:287–289
29. Baldissera P, Delprete C (2009) Effects of deep cryogenic treatment on static mechanical properties of 18NiCrMo5 carburized steel. Mater Des 30(5):1435–1440. https://doi.org/10.1016/j.matdes.2008.08.015
30. Yan D, Hilditch T, Kishawy H, Littlefair G (2013) On quantifying the strain rate during chip formation when machining aerospace alloy Ti-5553. Procedia CIRP 8:123–128. https://doi.org/10.1016/j.procir.2013.06.076
31. Filip R, Kubiak K, Ziaja W, Sieniawski J (2003) The effect of microstructure on the mechanical properties of two-phase titanium alloys. J Mater Process Technol 133(1-2):84–89. https://doi.org/10.1016/S0924-0136(02)00248-0
32. Oxley PLB, Young HT (1990) The mechanics of machining: an analytical approach to assessing machinability. Ellis Horwood Publisher, Chichester
33. Waldorf DJ, DeVor RE, Kapoor SG (1998) A slip-line field for ploughing during orthogonal cutting. J Manuf Sci Eng 120(4):693–699. https://doi.org/10.1115/1.2830208
34. Shaw M, Vyas A (1993) Chip formation in the machining of hardened steel. CIRP ANN-Manuf Technol 42(1):29–33. https://doi.org/10.1016/S0007-8506(07)62385-3
35. Wang B, Liu Z (2014) Investigations on the chip formation mechanism and shear localization sensitivity of high-speed machining Ti6Al4V. Int J Adv Manuf Technol 75(5-8):1065–1076. https://doi.org/10.1007/s00170-014-6191-y
36. Hua J, Shivpuri R (2004) Prediction of chip morphology and segmentation during the machining of titanium alloys. J Mater Process Technol 150(1-2):124–133. https://doi.org/10.1016/j.jmatprotec.2004.01.028
37. Yildiz Y, Nalbant M (2008) A review of cryogenic cooling in machining processes. Int J Mach Tools Manuf 48(9):947–964. https://doi.org/10.1016/j.ijmachtools.2008.01.008
38. Özel T, Karpat Y (2005) Predictive modeling of surface roughness and tool wear in hard turning using regression and neural networks. Int J Mach Tools Manuf 45(4-5):467–479. https://doi.org/10.1016/j.ijmachtools.2004.09.007
39. Nakayama K, Arai M (1987) Burr formation in metal cutting. CIRP ANN-Manuf Technol 36(1):33–36. https://doi.org/10.1016/S0007-8506(07)62547-5
40. Gaitonde V, Karnik S, Achyutha B, Siddeswarappa B (2008) Genetic algorithm-based burr size minimization in drilling of AISI 316L stainless steel. J Mater Process Technol 197(1-3):225–236. https://doi.org/10.1016/j.jmatprotec.2007.06.029